HAL open science

Synthesis and electronic properties of bridged [8]-, [12]- and [16]-cyclo-para-phenylenes

Fabien Lucas, Joëlle Rault-Berthelot, Cassandre Quinton, Cyril Poriel

To cite this version:

Fabien Lucas, Joëlle Rault-Berthelot, Cassandre Quinton, Cyril Poriel. Synthesis and electronic properties of bridged [8]-, [12]- and [16]-cyclo-para-phenylenes. Journal of Materials Chemistry C, 2022, 10, pp.14000-14009. 10.1039/d2tc00881e . hal-03798111

HAL Id: hal-03798111

https://hal.science/hal-03798111v1

Submitted on 5 Oct 2022

HAL is a multi-disciplinary open access archive for the deposit and dissemination of scientific research documents, whether they are published or not. The documents may come from teaching and research institutions in France or abroad, or from public or private research centers.

L'archive ouverte pluridisciplinaire **HAL**, est destinée au dépôt et à la diffusion de documents scientifiques de niveau recherche, publiés ou non, émanant des établissements d'enseignement et de recherche français ou étrangers, des laboratoires publics ou privés.

Distributed under a Creative Commons Attribution - NonCommercial 4.0 International License

Journal of Materials Chemistry C

ROYAL SOCIETY OF CHEMISTRY

PAPER

View Article Online
View Journal | View Issue

Open Access Article. Published on 12 September 2022. Downloaded on 10/5/2022 9:01:52 AM.
This article is licensed under a Creative Commons Attribution-NonCommercial 3.0 Unported Licence.

Check for updates

Cite this: J. Mater. Chem. C, 2022, 10, 14000

Synthesis and electronic properties of bridged [8]-, [12]- and [16]-cyclo-*para*-phenylenes†

Fabien Lucas, Joëlle Rault-Berthelot, Cassandre Quinton * and Cyril Poriel *

Received 3rd March 2022,
Accepted 15th August 2022

DOI: 10.1039/d2tc00881e

rsc.li/materials-c

Hoop-shaped π-conjugated macrocycles constitute a new family of π-conjugated systems displaying unique properties induced by their radially directed π-orbitals. The electronic properties of these nanohoops are deeply dependent on their building units and their size. We report herein the first size dependence study of [8]-, [12]- and [16] cyclo-*para*-phenylenes bridged by nitrogen atoms. The properties were elucidated by ^{1}H NMR, cyclic voltammetry, UV-vis absorption and fluorescence spectroscopy (in solution and in thin film). Thus, this work reports one of the largest bridged nanohoops synthesized, namely [4]cyclo-*para*-9-ethylhexyl-2,7-diphenyl-carbazole **[16]CPP4N**, an analog of **[16]CPP**, which displays an alternation of four unbridged biphenylenes and four nitrogen bridged biphenylenes. Removing either all the unbridged phenylenes ([4]cyclo-*para*-9-ethylhexyl-carbazole **[8]CPP4N**, an analog of **[8]CPP**) or one building unit ([3]cyclo-*para*-9-ethylhexyl-2,7-diphenyl-carbazole **[12]CPP3N**, an analog of **[12]CPP**) allows decreasing the size of the nanohoop with nevertheless drastically different consequences on the properties. This is what we aim at reporting in this work.

Introduction

In the last ten years, the properties of nanohoops have been the subject of intense research studies.[1–9] These types of studies appear to be of great interest firstly to rationalize and secondly to control the properties of this new family of π-conjugated systems possessing radially directed molecular orbitals. While most of these studies deal with small nanohoops, larger nanohoops such as those derived from **[16]CPP** remain barely studied,[10–17] even though some theoretical studies simulated interesting properties.[9,18,19] Furthermore, most of the studies dealing with the evolution of the properties of nanohoops upon size modification have been performed on cyclo-*para*-phenylenes (CPPs), the flagship family of nanohoops.[1,15,20–22] Bridged CPPs are a new generation of nanohoops recently reported in the literature.[23–32] Bridged CPPs are constructed on a CPP backbone in which two neighbouring phenylenes are linked through the *ortho* positions of the biphenyl bond by a common atom so that a five membered ring is formed. In organic semi-conductors (OSCs), bridging effects have been particularly studied and bridged linear π-conjugated systems have played a key role in the development of the emerging technology of organic electronics.[33–36] Indeed, in linear π-conjugated systems, the bridge rigidifies the molecular structure and drastically changes the electronic and physical properties in comparison to unbridged structures.[35–40] In the emerging field of nanohoops, the exact role of the bridge (which can be either a carbon,[23–28] sulfur[29] or nitrogen[30–32] atom) in the tuning of the electronic properties still remains unclear. In particular, the property evolution as a function of the size in bridged CPPs remains to be elucidated. In the nanohoop research field, cyclocarbazoles have recently attracted increased interest as they constitute the first family of nanohoops, which have been successfully

Univ Rennes, CNRS, ISCR-UMR 6226, F-35000 Rennes, France.
E-mail: Cyril.poriel@univ-rennes1.fr, cassandre.quinton@univ-rennes1.fr

† Electronic supplementary information (ESI) available: General experimental methods, synthetic procedures, 1D and 2D NMR spectra, electrochemical studies, photophysical studies, and theoretical properties. See DOI: https://doi.org/10.1039/d2tc00881e

Cassandre Quinton

Dr Cassandre Quinton is a CNRS researcher working in the field of π-conjugated materials (nanohoops, bridged oligophenylenes, etc.). She received her PhD in Chemistry from the Ecole Normale Supérieure de Cachan. After that, she obtained a postdoctoral fellowship from the Japan Society for the Promotion of Science to conduct her research at the Nara Institute of Science and Technology. In 2016, she was awarded a Marie Skłodowska-Curie Individual Fellowship to start her research on nanohoops at the University of Rennes 1. In 2018, she joined the CNRS. Her current molecules of interest are cyclic bridged oligophenylenes.

 This journal is © The Royal Society of Chemistry 2022

Open Access Article. Published on 12 September 2022. Downloaded on 10/5/2022 9:01:52 AM.
This article is licensed under a Creative Commons Attribution-NonCommercial 3.0 Unported Licence.

incorporated into a p-type organic field-effect transistor, showing the possibility of using such a type of macrocycles in organic electronic devices.[31,32] Furthermore, in 2019, it has been shown, using theoretical calculations, that the mobility of CPPs may increase with the nanohoop size.[41]

In the present work, we report one of the largest bridged nanohoops reported to date: [4]cyclo-*para*-9-ethylhexyl-2,7-diphenyl-carbazole **[16]CPP4N**, which possesses 16 phenylenes and 4 nitrogen bridges. In order to evaluate the influence of the size and the rigidity of the nanohoop on its electronic properties, a key feature of an OSC, we also report two other nanohoops displaying a different number of phenylenes and bridges: [3]cyclo-*para*-9-ethylhexyl-2,7-diphenyl-carbazole **[12]CPP3N**, which possesses 12 phenylenes and 3 nitrogen bridges, and [4]cyclo-*para*-9-ethylhexyl-carbazole **[8]CPP4N**, which possesses 8 phenylenes and 4 nitrogen bridges. Note that all the phenylenes of **[8]CPP4N** are substituted by nitrogen atoms whereas only half of phenylenes of **[12]CPP3N** and **[16]CPP4N** are bridged. Thus, the smallest nanohoop **[8]CPP4N** belongs to the family of the bridged nanohoops and the larger ones **[12]CPP3N** and **[16]CPP4N** will be called hybrid nanohoops, composed of bridged phenylenes (like bridged nanohoops) and unbridged phenylenes (like CPPs), in which the building unit is a carbazole-biphenylene.

This study reports the synthesis of these three nanohoops and the consequences of the size decrease of **[16]CPP4N** on the ^{1}H NMR, electrochemical and spectroscopic properties (absorption and emission, stationary and time-resolved, in solution and in thin solid films). Two types of size decrease have been considered: (i) the removal of one building unit, *i.e.* two unbridged phenylenes and one carbazole, to give **[12]CPP3N** and (ii) the removal of all the unbridged phenylenes to give **[8]CPP4N** (Fig. 1). In the case of **[8]CPP4N**, the number of nitrogen bridges and the symmetry (D_{2d}) remain unchanged compared to **[16]CPP4N**, whereas **[12]CPP3N** displays only 3 nitrogen bridges and a lower symmetry (C_s). By comparing **[16]CPP4N** with its two smaller analogues **[12]CPP3N** and **[8]CPP4N**, we aim at shedding light on the most influent parameters involved in the modification of the electronic properties, which hold a major role in the performance of an OSC in a device.

Results and discussion

The synthesis of the three nanohoops was performed following the Pt approach initially developed by Yamago and coworkers in 2010[42] (Scheme 1), which was never employed to synthesize nanohoops as large as **[16]CPP** derivatives. First, the nitrogen atom of 2,7-dibromocarbazole was alkylated with a 2-ethylhexyl chain (EtHex) in order to ensure the solubility of the final compounds in organic solvents and was then functionalized with pinacolato boron units to give **1** (Schemes S1 and S2, ESI†). The phenylene spacers were then successfully introduced *via* a selective Suzuki–Miyaura cross-coupling involving 1-bromo-4-iodobenzene, potassium hydroxide and $PdCl_2$(dppf), providing **2** in a high yield of 91%. Compound **2** was then functionalized with pinacolato boron units to give the final nanohoop precursor **3**. The cyclization step follows an optimized procedure previously reported for a smaller bridged nanohoop.[31] The intermediates **4** and **5**, respectively based on four and three platinum complexes, were formed (not isolated) by stirring bis(pinacolato)diboron **3** with $PtCl_2$(cod) and cesium fluoride in a refluxing THF solution for 24 h. Then, the dried crude mixture containing **4** and **5** was treated with triphenylphosphine in *o*-dichlorobenzene, 1 h at room temperature and 48 h at 180 °C to provide the two sizes of nanohoops: **[16]CPP4N** (7% yield) and **[12]CPP3N** (3% yield) with respectively four and three building units connected.

In order to precisely study the size decrease effects of **[16]CPP4N**, keeping nevertheless the same number of carbazoles,

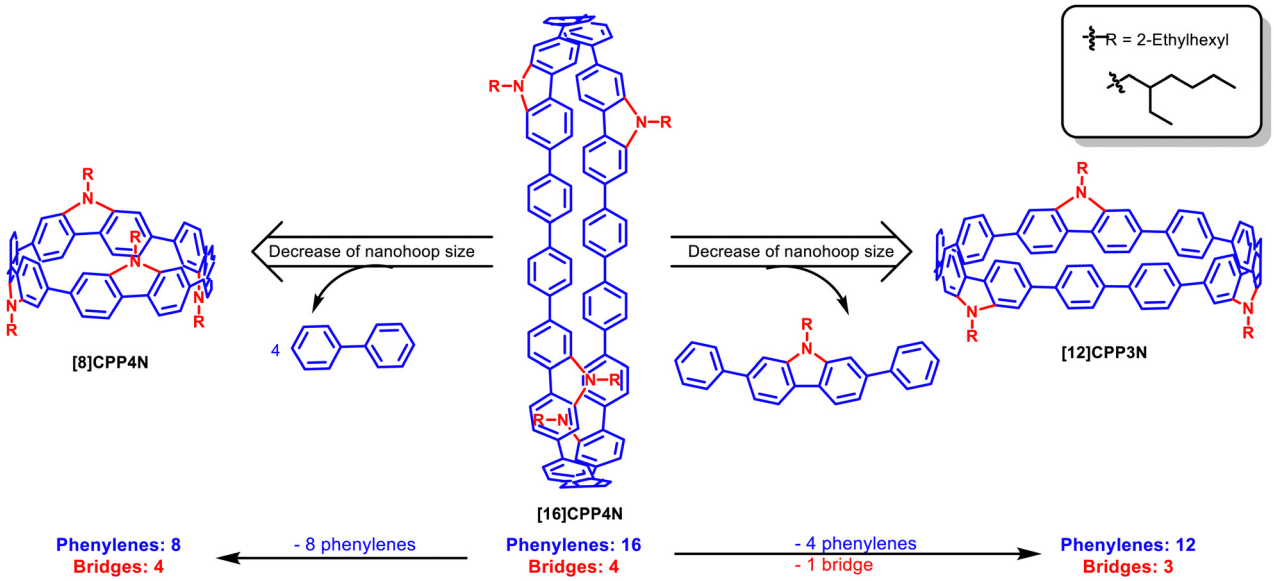

Fig. 1 Structures of **[8]CPP4N**, **[16]CPP4N** and **[12]CPP3N**.

Open Access Article. Published on 12 September 2022. Downloaded on 10/5/2022 9:01:52 AM.
This article is licensed under a Creative Commons Attribution-NonCommercial 3.0 Unported Licence.

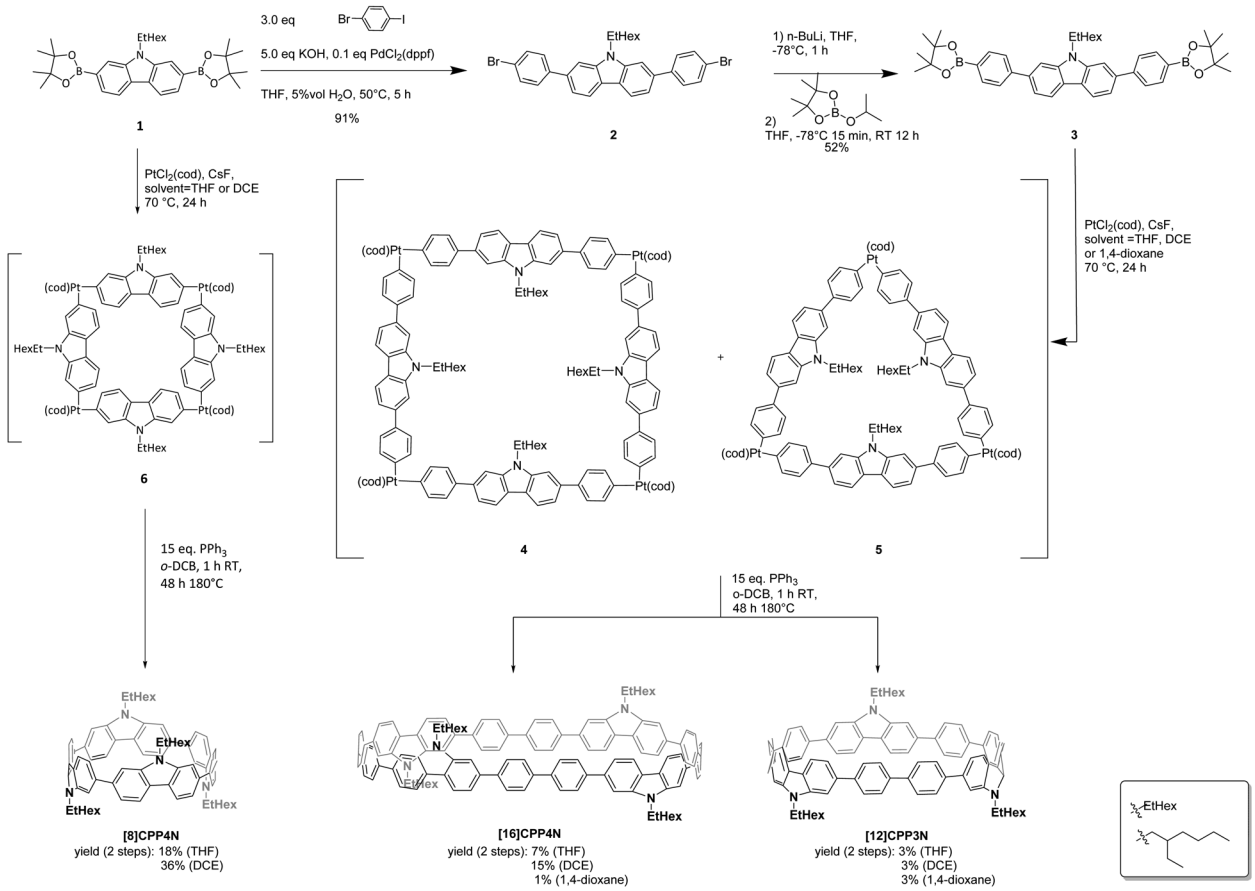

Scheme 1 Synthesis of **[8]CPP4N**, **[16]CPP4N** and **[12]CPP3N**.

[8]CPP4N was synthesized. Thus, following the same cyclization procedure, **[8]CPP4N** was successfully isolated with 18% yield from **1** (also used as an intermediate in the synthesis of the larger nanohoops). The yield of **[8]CPP4N** in the case of the cyclization from **1** (18%) is higher than that of **[16]CPP4N** in the case of the cyclization from **3** (7%). Thus, decreasing the size of the bis(pinacolato)diboron precursor leads to a higher yield. This synthetic consideration is identical to that observed in the case of CPPs: under the same conditions, two square-shaped tetra-nuclear platinum intermediates (respectively from a distannylated diphenyl/terphenyl leading to **[8]CPP**/**[12]CPP**) have been obtained with a yield of 37% and 11% respectively.[43] The higher yields obtained for the smaller precursors could be due to the higher solubility of their corresponding oligoaryl platinum complexes in THF, as previously reported in the case of large CPPs.[43] Thus, in order to improve the yield of the cyclization, the synthesis of the platinum intermediates **4** and **5** was performed in 1,4-dioxane and 1,2-dichloroethane (DCE) keeping all the other parameters (for both steps) unchanged (see above). In 1,4-dioxane, the yield of **[16]CPP4N** was only 1% whereas in DCE, it was significantly increased to 15%. Thus, the use of DCE allows doubling the initial total yield in THF (7% in THF → 15% in DCE). The same effect is also detected in the case of **[8]CPP4N** (18% in THF → 36% in DCE), showing that DCE in the transmetallation step is a highly efficient and versatile solvent (note that, in the purpose of this work, we also have investigated another alkyl chain, *i.e.* butyl, but failed to isolate **[12]CPP3N-Bu** and **[16]CPP4N-Bu**, the corresponding nanohoops displaying a butyl chain instead of the ethylhexyl chain, even using DCE as the solvent, showing the importance of the alkyl chain borne by the nitrogen atom on the solubility of the intermediaries). This finding appears as an important feature as synthetic considerations remain the cornerstone of the nanohoop research field.[32] It is nevertheless important to mention that this positive effect is only detected for 4-unit nanohoops as the yield of **[12]CPP3N** remains unchanged whatever the solvent used (3%). The presence of **[12]CPP3N** can be explained by the formation of the triangle-shaped tri-nuclear platinum intermediate **5**. This kind of triangular intermediate has already been reported for the synthesis of a cyclic trifluorene.[24] Note that in the case of **[8]CPP4N**, no 3-unit (or other *n*-unit) nanohoop was isolated. As the cyclization reactions of precursors **1** and **3** are performed under identical experimental conditions, the precursors themselves are undoubtedly at the origin of the different ratio of 3-unit *vs.* 4-unit nanohoops obtained. Thus, **3** is larger and more flexible than **1**, which helps the formation of the triangle intermediary.[44] Also, in a hypothetical triangle from **1**, the branched alkyl chains would induce an important steric hindrance whereas in the case of **5**, thanks to the phenylenes, they are far away one from another. This is why **3** can lead to the stabilized triangle **5** whereas **1** cannot give a

Open Access Article. Published on 12 September 2022. Downloaded on 10/5/2022 9:01:52 AM.
This article is licensed under a Creative Commons Attribution-NonCommercial 3.0 Unported Licence.

stable triangle. Thus, the size and flexibility of the bis(pinacolato) diboron precursor influences not only the yield of the cyclization step but also the number of units in the nanohoop. Therefore, compared to **1**, **3** leads to a lower yield but allows the formation of two sizes of nanohoops, **[12]CPP3N** and **[16]CPP4N** with three and four units respectively. As the relationship between the nanohoop size and its electronic and structural properties is a central notion,[1,9,20,21,23,43,45–51] reaching the unexpected **[12]CPP3N** appears to be an interesting synthetic feature.

In the aromatic region, the ^{1}H NMR of **[16]CPP4N** displays five signals (Fig. 2a), which have been attributed, thanks to 2D-COSY experiments (Fig. S15, ESI†), to Ha, Hb and Hc borne by the bridged phenylenes and Hd and He borne by the unbridged phenylenes. The singlet corresponding to Ha is the most upfield shifted signal (δ = 7.30 ppm) due to the ring current of the macrocycle.[30] **[12]CPP3N** displays a similar signature (Fig. 2b). Nevertheless, one can note that all the signals (except He) in **[12]CPP3N** are shielded compared to their homologues in **[16]CPP4N**. This is particularly marked for Ha, which displays a resonance at δ = 7.10 ppm. Thus, the decrease of the size of **[16]CPP4N** by removing a building unit (*i.e.* two unbridged phenylenes and one carbazole) induces an upfield shift. This phenomenon probably arises from the greater shielding from the individual phenylenes across the diameter of the smaller nanohoop and has previously been observed by varying the size of cyclofluorenes[23] or cyclo-*para*-phenylene-2,6-naphthylenes.[51] The same effect is not only observed when comparing **[16]CPP4N** and **[8]CPP4N** but also exacerbated. Indeed, by removing all the unbridged phenylenes, Ha is significantly shielded to 6.52 ppm (Fig. 2c). [*n*]CPPs follow the same size rules in NMR spectroscopy.[1,43] Removing all the unbridged phenylenes also leads to an upfield shift of Hb and Hc resonances. In summary, the decrease of the size from **[16]CPP4N** to **[12]CPP3N** or to **[8]CPP4N** induces an upfield shift of the bridged phenylene signals, this shift being more pronounced for the smallest nanohoop **[8]CPP4N**, most likely due to the fact that the smaller the nanohoop size, the higher the ring current[30,52] and the magnetic shielding effect.

Electrochemical analyses of **[16]CPP4N**, **[12]CPP3N** and **[8]CPP4N** were performed by cyclic voltammetry (CV) in *N*,*N*-dimethylformamide (DMF) for the cathodic explorations and in 1,1,2,2-tetrachloroethane (TCE) for the anodic explorations (classical dichloromethane could not be used herein due to solubility reasons). Results are gathered in Table 1. In oxidation (Fig. 3a), both **[16]CPP4N** and **[12]CPP3N** display irreversible processes with shoulders (sh) around 0.6 and 0.7 V and a maximum at 0.91 V for the former and a maximum at 0.99 V for the latter, whereas **[8]CPP4N** presents a first reversible wave with a maximum at 0.40 V. For the three compounds, additional oxidation waves are recorded at more positive potentials (Fig. S33, ESI† and Table 1). The irreversibility of the first oxidation wave of both **[16]CPP4N** and **[12]CPP3N** translates the high reactivity of the charged species generated upon the first oxidation, which leads to carbon–carbon couplings. As previously reported, we believe that C–C couplings occur at C3/C6 positions of the carbazole unit.[53–55] Thus electrodeposition of insoluble species are electrodeposited on the platinum surface (details are provided in Fig. S34–S36, ESI†). The HOMO energy levels of **[16]CPP4N** and **[12]CPP3N**, measured from the threshold potential of their first oxidation, appear similar (−5.25 and −5.31 eV, respectively), whereas the HOMO of **[8]CPP4N** is significantly higher (−5.09 eV). This is in agreement with a theoretical study performed on [*n*]CPPs,[43] which shows that the decrease of the HOMO level is significant

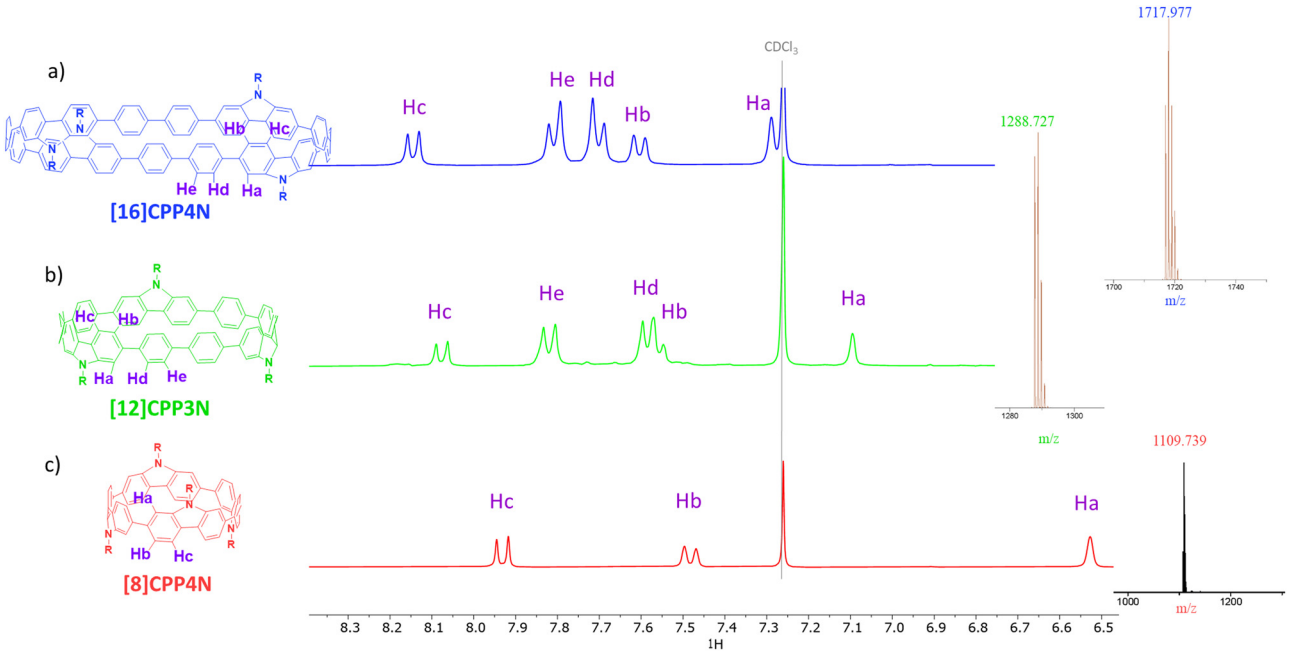

Fig. 2 Parts of the ^{1}H NMR ($CDCl_3$) and mass spectra of (a) **[16]CPP4N** in blue, (b) **[12]CPP3N** in green and (c) **[8]CPP4N** in red (full spectra in ESI†).

Open Access Article. Published on 12 September 2022. Downloaded on 10/5/2022 9:01:52 AM.
This article is licensed under a Creative Commons Attribution-NonCommercial 3.0 Unported Licence.

Table 1 Electrochemical, photophysical and theoretical properties

	Solvent	[16]CPP4N	[12]CPP3N	[8]CPP4N
E^{ox} [V]	TCE	0.60 (sh), 0.70 (sh), 0.91	0.99	0.40, 1.20 (sh)
E^{ox}_{onset} [V]		0.45	0.51	0.29
E^{red} [V]	DMF	−3.05	−2.64 (sh)	−2.68 (sh)
E^{red}_{onset} [V]		−2.54	−2.43	−2.55
HOMO [eV][a]	TCE	−5.25	−5.31	−5.09
LUMO [eV][a]	DMF	−2.26	−2.37	−2.25
λ_{abs} [nm] ($\varepsilon \times 10^5$ [L mol^{-1} cm^{-1}], FWHM [nm])	$CHCl_3$	350 (2.8, 54)	347 (1.8, 51)	341 (0.93, 42)
λ_{em} [nm] (FWHM [nm])		419, 439 (54)	432, 452 (67)	492 (86)
QY[b]		0.76	0.71	0.21
τ [ns][c]		2.0 (12%), 1.0 (88%)	2.2 (83%),1.1 (17%)	6.4 (93%), 3.3 (7%)
k_r [ns^{-1}][d]		0.76	0.32	0.03
k_{nr} [ns^{-1}][d]		0.24	0.13	0.12
λ_{abs} [nm] ($\varepsilon \times 10^5$ [L mol^{-1} cm^{-1}])	Cyclohexane	344	342	339 (0.92)
λ_{em} [nm]		413, 436 (sh)	422, 441	485
QY[b]		0.79	0.80	0.20
τ [ns][e]		2.0 (17%), 1.0 (83%)	2.1 (85%),1.0 (15%)	6.5
k_r [ns^{-1}][d]		0.79	0.38	0.03
k_{nr} [ns^{-1}][d]		0.21	0.10	0.12
$\lambda_{abs,film}$ [nm]	Film[f]	386	354	347
$\lambda_{em,film}$ [nm]		435, 459	445, 465	491
QY_{film}		0.10	0.04	0.16
HOMO [eV][g]	Vacuum	−5.12	−5.04	−4.89
LUMO[eV][g]		−1.55	−1.63	−1.36

[a] Calculated from the onset potentials: HOMO (eV) = $-[E^{ox}_{onset}$ (*vs.* Fc/Fc$^+$) + 4.8] and LUMO (eV) = $-[E^{red}_{onset}$ (*vs.* Fc/Fc$^+$) + 4.8]. [b] Using quinine sulfate in 0.5 M (QY = 0.54) as a reference. [c] λ_{exc} = 310 nm, λ_{em}(**[16]CPP4N**) = 440 nm, λ_{em}(**[12]CPP3N**) = 450 nm, λ_{em}(**[8]CPP4N**) = 500 nm. [d] Calculated with the dominant lifetime. [e] λ_{exc} = 310 nm, λ_{em}(**[16]CPP4N**) = 440 nm, λ_{em}(**[12]CPP3N**) = 450 nm, λ_{em}(**[8]CPP4N**) = 486 nm. [f] Spin-coated thin film from 1 mg mL^{-1} in THF solution. [g] DFT (b3lyp, 6-31g(d)), sh: shoulder.

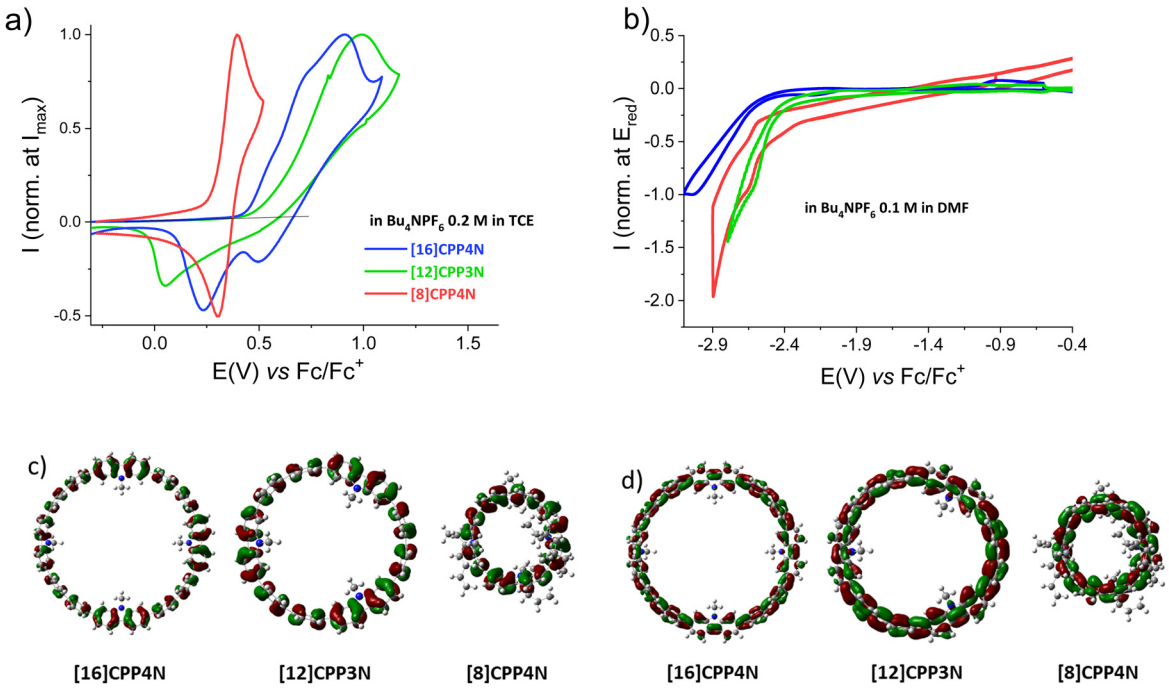

Fig. 3 Cyclic voltammograms of **[16]CPP4N** in blue, **[12]CPP3N** in green and **[8]CPP4N** in red with the Pt working electrode, sweep-rate 100 mV s^{-1} (a) in oxidation, $C_2H_2Cl_4$ + Bu_4NPF_6, 0.2 M, 100 mV s^{-1}, (b) in reduction, DMF + Bu_4NPF_6, 0.1 M, 100 mV s^{-1} and representation of (c) the HOMO and (d) the LUMO (b3lyp, 6-31g(d), shown with an isovalue of 0.02; alkyl chains have been shortened due to calculations resources.

when the size increases from **[4]CPP** to **[12]CPP** but becomes smaller for higher CPP sizes. It is interesting to note that **[12]CPP3N** also contains 12 phenylenes (as for **[12]CPP**), indicating therefore that this might be a threshold in the HOMO level evolution. Thus, decreasing the size of **[16]CPP4N** by removing one building unit does not affect significantly the

Open Access Article. Published on 12 September 2022. Downloaded on 10/5/2022 9:01:52 AM.
This article is licensed under a Creative Commons Attribution-NonCommercial 3.0 Unported Licence.

HOMO level whereas removing the unbridged phenylenes lead to a drastically different behaviour. Indeed, the first wave of **[8]CPP4N** is (i) recorded at a significantly lower potential of 0.40 V (corresponding to a higher HOMO energy of −5.09 eV) and (ii) is reversible. These two features need to be clarified. The increase of the HOMO energy level when all the unbridged phenylenes of **[16]CPP4N** are removed to give **[8]CPP4N** can be related to two effects. First, it is known that the decrease of the whole number of phenylenes induces an increase of the HOMO levels in the CPPs[43] series due to an increase of the orbital overlap. This evolution is induced in a benzenoidal HOMO (Fig. 3c) by the decrease of the torsion angles between the phenylenes (from 26.7° to 21.2° in the optimized geometries of the most stable conformers, see Fig. S57, S58 and Table S2, ESI†), which is a consequence of the strain.[15] Second, **[8]CPP** displays a HOMO energy level of −5.28 eV,[32] lower than that of **[8]CPP4N**: −5.09 eV. However, as the HOMO of **[8]CPP** was measured in CH_2Cl_2 in the previous work,[32] the HOMO of **[8]CPP4N** was also measured in CH_2Cl_2 and is shifted to −5.20 eV still remaining higher than that of **[8]CPP** (see Fig. S37, ESI†). As **[8]CPP4N** and **[8]CPP** possess both 8 phenylenes, the difference can be assigned to the electron rich character of the nitrogen bridges. This is in agreement with the HOMO levels of −5.16 and −5.23 eV simulated respectively for **[8]CPP4N** and **[8]CPP** both in the optimized geometry of **[8]CPP4N** (Fig. S60 and Table S3, ESI†). We propose that the mix between the orbitals of the electron-poor unbridged phenylenes and the electron-rich carbazoles in **[16]CPP4N** could decrease the HOMO energy level compared to **[8]CPP4N**, only constituted of electron-rich carbazoles. Note that the effect of the carbazoles on the HOMO level can also been observed by the comparison of **[12]CPP3N** (HOMO = −5.31 eV) and **[12]CPP** (HOMO = −5.5 eV measured using a similar method from Fig. 5 of ref. 43).

Concerning the reversibility of the first oxidation process, the cation-radical seems to be more stabilized on the small nanohoop (with 8 phenylenes) than on the larger nanohoops (with 12 or 16 phenylenes). The stability of the cation-radical is more influenced by the total number of phenylenes than by the number of donor nitrogen bridges. Yamago *et al.* also observed that the cation-radicals of CPPs become less stable when increasing the size for a series of CPPs.[43] Thus, removing all the unbridged phenylenes of **[16]CPP4N** to give **[8]CPP4N** induces a decrease of the HOMO and the generation of stable charged species at the electrode upon oxidation. To sum up, the two ways of decreasing the size of **[16]CPP4N** have drastically different consequences on the anodic properties. Removing one building unit (**[16]CPP4N** *vs.* **[12]CPP3N**) does not affect its oxidation properties while removing all the unbridged phenylenes (**[16]CPP4N** *vs.* **[8]CPP4N**) has a strong effect on it.

In reduction, the process is irreversible for the three nanohoops (Fig. 3b). A peak at −3.05 V is pointed for **[16]CPP4N** whereas shoulders are detected at −2.64 V for **[12]CPP3N** and at −2.68 V for **[8]CPP4N**. The LUMO levels have been estimated from the onset potentials of the reduction wave at −2.26, −2.37 and −2.25 eV, respectively. Thus, the LUMO of the largest nanohoop **[16]CPP4N** (−2.26 eV) is higher than that of **[12]CPP3N** (−2.37 eV). This trend is identical to that previously made for the CPPs family[23,56] and is linked to the quinoidal shape of the LUMO (Fig. 3d). This trend is due to the evolution of both the torsion angles and the displacement angles. Indeed, the average torsion angle is higher for the largest nanohoop (26.7° for **[16]CPP4N** *vs.* 23.1° for **[12]CPP3N** in their optimized geometries, see Fig. S57, S58 and Table S2, ESI†). Furthermore, the average displacement angle is lower for the largest nanohoop (7.4° for **[16]CPP4N** *vs.* 10.8° for **[12]CPP3N** in their optimized geometries, see Fig. S57, S59 and Table S2, ESI†). Remarkably, removing all the unbridged phenylenes has almost no impact on the LUMO energy levels, which appear to be almost identical for **[16]CPP4N** and **[8]CPP4N** (−2.26 and −2.25 eV). Two effects might be balanced. First, the increase of the total number of phenylenes should induce an increase of the LUMO level as observed above for **[12]CPP3N** and **[16]CPP4N**. Second, the mix between the orbitals of the unbridged phenylenes and those of the phenylenes bridged by a donor nitrogen atom in **[16]CPP4N** should in principle induce a decrease of the LUMO level compared to **[8]CPP4N**, only built on donor carbazoles. The compensation of these two effects could explain why the LUMO level remains constant when removing the unbridged phenylenes of **[16]CPP4N** to give **[8]CPP4N**. As a conclusion of the electrochemical part, the decrease of the size of **[16]CPP4N** by removing one building unit to give **[12]CPP3N** mainly affects the reduction properties whereas removing all the unbridged phenylenes of **[16]CPP4N** to give **[8]CPP4N** mainly affects the oxidation properties. This is a key feature in the design of nanohoop-based OSCs, which are now more and more required in the light of recent findings in the field of organic electronics.[25,31,32,57–59]

The spectroscopic properties of the three nanohoops have been studied in chloroform for solubility considerations (Table 1). The three nanohoops display the usual absorption characteristics (Fig. 4a, dashed line) found for nanohoops *i.e.* a band tail at around 400 nm, an intense band between 341 and 350 nm and other bands at higher energy. Whatever the removed units from **[16]CPP4N** (either all unbridged phenylenes to give **[8]CPP4N** or one carbazole and two unbridged phenylenes to give **[12]CPP3N**), three effects on the main band are observed: (i) its molar extinction coefficient decreases, (ii) its full width at half maximum (FWHM) decreases and (iii) it is blue-shifted. These effects are more pronounced when all the unbridged phenylenes are removed (in **[8]CPP4N**) than when a building unit is removed (in **[12]CPP3N**). The decreases of both molar extinction coefficient and FWHM from **[16]CPP4N** to **[12]CPP3N** can be directly correlated with the total number of building units in the nanohoops as also highlighted in the CPPs family.[15,43,60] The same tendency also observed from **[16]CPP4N** to **[8]CPP4N**, both containing four carbazole units, is directly linked to the presence/absence of unbridged phenylenes. The largest FWHM observed for **[16]CPP4N** can be attributed to inhomogeneous broadening due to high conformational structural variations. When decreasing its size, the number of ground state conformers (due to irregular variations of the dihedral angles between

Open Access Article. Published on 12 September 2022. Downloaded on 10/5/2022 9:01:52 AM.
This article is licensed under a Creative Commons Attribution-NonCommercial 3.0 Unported Licence.

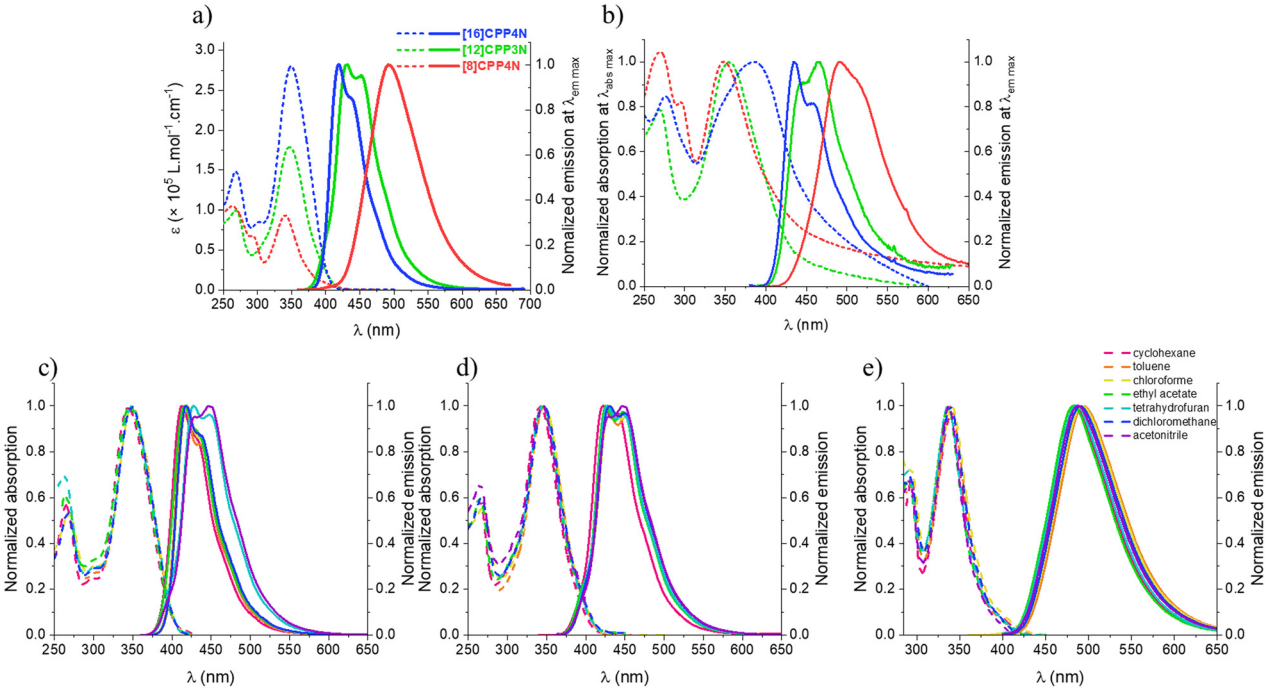

Fig. 4 Absorption (dashed line) and emission (solid line) spectra of **[16]CPP4N** in blue, **[12]CPP3N** in green and **[8]CPP4N** in red (a) in chloroform (b) in thin solid film (spin-coating of 1 mg mL^{-1} solution in THF). Absorption (dashed line) and emission (solid line) spectra in cyclohexane (pink), toluene (orange), chloroform (yellow), ethyl acetate (green), tetrahydrofuran (blue), dichloromethane (dark blue), acetonitrile (purple) of (c) **[16]CPP4N**, (d) **[12]CPP3N** and (e) **[8]CPP4N**.

the phenylenes) also decreases. The blue-shift of the main band when decreasing the size is not observed for the CPP family (no dependence of this band upon size modification) but has been previously reported for another family of bridged CPPs, namely cyclofluorenes from 5 to 4 units.[23] Thus, despite **[16]CPP4N** and **[12]CPP3N** being hybrid nanohoops displaying only one bridged biphenylene over two biphenylenes, they behave more as bridged CPPs than as CPPs regarding the evolution of the position of the absorption band upon size. This blue-shift is obviously more pronounced when comparing **[16]CPP4N** and **[8]CPP4N** for which all the phenylenes are bridged. Indeed, the building unit in **[8]CPP4N** is different from that in hybrid nanohoops and FWHM can also be influenced by the proportion of unbridged phenylenes/bridged phenylenes.

In emission spectroscopy (Fig. 4a, solid line), **[16]CPP4N** and **[12]CPP3N** display structured spectra with maxima at 419 and 439 nm for the former and at 432 and 452 nm for the latter whereas the spectrum of **[8]CPP4N** is large and unstructured with a maximum at 492 nm. Thus, decreasing the size of **[16]CPP4N** induces a significant red-shift, whatever the removed units. Such a behaviour is similar to that described for CPPs[20] and bridged CPPs.[23] This is due to an increase in the orbital overlap (which therefore increase the π-conjugation) in the small strained nanohoops, as discussed in the electrochemical part. Furthermore, the structuration of the emission band observed for the large nanohoops **[16]CPP4N** and **[12]CPP3N** is also observed for their unbridged analogues **[12]CPP** and **[16]CPP**[15] but not for the smaller **[8]CPP**[20] and **[8]CPP4N**. Thus, the shape of the emission band seems to be more correlated with the total number of phenylenes than to the presence of bridges. In fact, the smaller nanohoops are more bent, which increases the number of vibrational modes and thus broadens the band.[60] Therefore, the FWHM increases when decreasing the size (54, 67 and 86 nm respectively for **[16]CPP4N**, **[12]CPP3N** and **[8]CPP4N**), in contrast to what was observed in absorption (see above). **[16]CPP4N** and **[12]CPP3N** possess identical quantum yields (*ca.* 0.7) and similar fluorescence lifetimes (*ca.* 1 and 2 ns). In contrast, removing all the unbridged phenylenes, *i.e.* going from **[16]CPP4N** to **[8]CPP4N**, induces an important decrease of the quantum yield (0.8 *vs.* 0.2) and an increase of the fluorescence lifetime (1.0 *vs.* 6.4 ns). The radiative rate constants k_r of **[16]CPP4N** and **[12]CPP3N** (0.76 and 0.32 ns^{-1}) are one order of magnitude higher than that of **[8]CPP4N** (0.03 ns^{-1}) whereas the non-radiative constants k_{nr} are similar for the three nanohoops (0.12–0.24 ns^{-1}). Therefore, the lower quantum yield of **[8]CPP4N** compared to the ones of the larger nanohoops is caused by much lower electronic transition moments and not by more efficient internal conversion processes. This is different from what might have been imagined at first glance; *i.e.* the unbridged phenylenes add some flexibility and then increase non-radiative processes. In CPPs series, **[16]CPP** displays the same quantum yield as **[12]CPP** (*ca.* 0.88) whereas it drops down in **[8]CPP** (0.25).[15,20] Also, the quantum yields of **[16]CPP**, **[12]CPP** and **[8]CPP** are close to the ones of **[16]CPP4N**, **[12]CPP3N** and **[8]CPP4N**, respectively. Thus, the evolution of the quantum yield in these bridged nanohoops seems to be more driven by the number of phenylenes than by the presence of the bridges.

In thin solid films, the absorption spectra of **[16]CPP4N**, **[12]CPP3N** and **[8]CPP4N** display a maximum at 386, 354 and

Open Access Article. Published on 12 September 2022. Downloaded on 10/5/2022 9:01:52 AM.
This article is licensed under a Creative Commons Attribution-NonCommercial 3.0 Unported Licence.

347 nm respectively (Fig. 4b, dashed line). First, the evolution of the position of the main absorption band upon design modification remains unchanged compared to the study in solution. Second, the bathochromic shift observed from the solution in cyclohexane to the thin film is 42 nm for the largest **[16]CPP4N** and only 12 nm for the two smallest nanohoops **[12]CPP3N** and **[8]CPP4N**. We assume that the larger shift observed for **[16]CPP4N** is due to intermolecular interactions at the solid state. The broadening of the absorption spectrum of **[16]CPP4N** is in accordance with these conclusions. Note also that the absorption between 450 and 500 nm is increased in the films compared to in solution. This is more obvious for **[16]CPP4N** than for **[12]CPP3N** than for **[8]CPP4N**. By reducing the size of the nanohoop (whatever the removed unit), the intermolecular interactions are highly reduced. In thin film emission (Fig. 4b, solid line), **[16]CPP4N** and **[12]CPP3N** display structured spectra with maxima at 435 and 459 nm for the former and at 445 and 465 nm for the latter whereas the spectrum of **[8]CPP4N** is large and unstructured with a maximum at 491 nm. As observed in absorption, the evolution of the position of the main fluorescence band upon design modification remains unchanged compared to the study in solution. The bathochromic shift observed from the solution in cyclohexane to the thin solid film is *ca.* 22 and 23 nm for **[16]CPP4N** and **[12]CPP3N** respectively and only 6 nm for **[8]CPP4N**. Note that this shift is 20 nm for **[8]CPP**, showing that the nitrogen bridges with the sterically hindered alkyl chains allow limiting the aggregation. Furthermore, the quantum yields are 0.10 for **[16]CPP4N**, 0.04 for **[12]CPP3N** and 0.16 for **[8]CPP4N**. Thus, decreasing the size of **[16]CPP4N** by removing a building unit induces a decrease of the quantum yield at the solid state whereas removing all the unbridged phenylenes induces an increase of the quantum yield. From solution to solid state, the quantum yields of **[16]CPP4N** and **[12]CPP3N** are divided by around 10 and 20 respectively, while the quantum yield of **[8]CPP4N** remains almost unchanged. Thus, both **[16]CPP4N** and **[12]CPP3N** seem to display some intermolecular interactions responsible for both the bathochromic shift from the solution to the solid state and the decrease of the quantum yield between the solution and the solid state. In contrast, in **[8]CPP4N**, removing all the unbridged phenylenes prevents any intermolecular interactions and the photophysical properties in solution are roughly maintained in the solid state. Thus, the unbridged phenylenes in the large nanohoops are surely involved in intermolecular interactions, which affect the QY in the solid state. Indeed, the hybrid nanohoops display unbridged phenylenes which are more accessible to be involved in intermolecular interactions than the bridged ones which are sterically hindered with the alkyl chain. This finding appears to be particularly important for further optoelectronic applications.

Solvatochromic experiments have also been performed. We first note that the absorption maxima of the three nanohoops are almost insensitive to the environment (Fig. 4c–e, dashed lines). As is often observed, the emission spectra are more influenced by the nature of the solvent, although herein this influence remains modest. Indeed, for **[16]CPP4N**, there is a bathochromic shift of 18 nm from the less polar cyclohexane to the more polar acetonitrile (Fig. 4c and Table S1, ESI†). This bathochromic shift is the consequence of the stabilization of the emissive state by the polar solvent, leading to an energy gap contraction. This is caused by dipole–dipole interactions between the nanohoops and polar solvent molecules. Note that some other characteristics of the solvents (such as their nucleophilic, electrophilic, acidic and basic properties) may significantly contribute to the stabilization of the emissive state (which explains why the emission wavelength in ethyl acetate is low despite its high polarity). For **[12]CPP3N**, this shift is of only 9 nm (Fig. 4d and Table S1, ESI†) showing that removing one building unit significantly decreases these stabilizing interactions, and notably the dipole–dipole interactions. As it is known that photophysics of donor–acceptor biphenylenes strongly depends on the torsion angle,[61] the difference observed between **[16]CPP4N** and **[12]CPP3N** can also be tentatively assigned to the different structural arrangements between bridged and unbridged phenylenes induced by their different symmetry and strain. Finally, the emission of **[8]CPP4N** is not influenced by the polarity of the solvent (Fig. 4e and Table S1, ESI†). This feature translates that removing all the unbridged phenylenes does not allow to stabilize the emissive state. The strain, which is really higher in **[8]CPP4N** than in the hybrid nanohoops, could be at the origin of this destabilization of the excited state. Thus, solvatofluorochromism was observed in both **[12]CPP3N** and **[16]CPP4N**. Therefore, the incorporation of nitrogen bridges in a CPP induces a stabilization of the emissive state by some polar solvents particularly important compared to cyclohexane, which can be modulated by the number of bridges in the nanohoop.

Conclusions

In summary, we reported the synthesis, and the ^{1}H NMR, electrochemical and photophysical properties of a large hybrid nanohoop **[16]CPP4N** and its smaller analogs **[12]CPP3N** and **[8]CPP4N**. We have shown that the size (and the resulting flexibility) of the bis(pinacolato)diboron precursor of nanohoops influences not only the yield of the cyclization step but also the number of building units within the nanohoop. This is an interesting feature to synthesize the nanohoop with three building units **[12]CPP3N**. The decrease of the size of **[16]CPP4N** by removing one building unit to give **[12]CPP3N** mainly affects the reduction properties whereas removing all unbridged phenylenes of **[16]CPP4N** to give **[8]CPP4N** mainly affect the oxidation properties. This feature could be used to design nanohoop-based OSCs with HOMO/LUMO levels fitting a desired application. The evolution of the absorption properties in solution upon size is specific to bridged CPPs whereas the evolution of the fluorescence properties follows the rules defined for CPPs. Removing all unbridged phenylenes of **[16]CPP4N** is efficient for reducing the intermolecular interactions in the solid state, which is a key parameter for optoelectronic applications. Furthermore, the three present bridged nanohoops display specific properties compared to those of CPPs (higher HOMO

Open Access Article. Published on 12 September 2022. Downloaded on 10/5/2022 9:01:52 AM.
This article is licensed under a Creative Commons Attribution-NonCommercial 3.0 Unported Licence.

level and weaker aggregation). For all the nanohoop families and especially those constructed on different building units, defining the evolution of their electronic properties as a function of both the nanohoop size and the building units is a crucial step in the understanding of these new generations of π-conjugated systems. As nanohoops are now entering in the era of applications,[32,62] these findings may be used to further design functional materials for organic electronics. We are currently working in this direction.

Conflicts of interest

There are no conflicts to declare.

Acknowledgements

This project has received funding from the European Union's Horizon 2020 research and innovation program under grant agreement No 699648 (FRODO Project). The authors would like to thank the Région Bretagne (DIADEM project) for PhD grant (FL) and Rennes Métropole for the Allocation d'Installation Scientifique (NADEO project). We would like to thank the CRMPO (Rennes) for mass analysis. We thank GENCI (Project N° AD010805032R1) and Dr G. Clavier for allocation of computational time.

References

1 E. R. Darzi and R. Jasti, *Chem. Soc. Rev.*, 2015, **44**, 6401–6410.
2 S. Yamago, E. Kayahara and S. Hashimoto, *Polycyclic Arenes and Heteroarenes*, 2015, pp. 143–162.
3 Y. Xu and M. von Delius, *Angew. Chem., Int. Ed.*, 2020, **59**, 559–573.
4 D. Wu, W. Cheng, X. Ban and J. Xia, *Asian J. Org. Chem.*, 2018, **7**, 2161–2181.
5 M. Hermann, D. Wassy and B. Esser, *Angew. Chem., Int. Ed.*, 2021, **60**, 15743–15766.
6 D. Lu, Q. Huang, S. Wang, J. Wang, P. Huang and P. Du, *Front. Chem.*, 2019, **7**, 668.
7 S. E. Lewis, *Chem. Soc. Rev.*, 2015, **44**, 2221–2304.
8 H. Chen, M. R. Golder, F. Wang, R. Jasti and A. K. Swan, *Carbon*, 2014, **67**, 203–213.
9 L. Wang, S.-H. Chen, D. He, Q.-J. Li, Y.-L. Liu and M.-S. Wang, *J. Phys. Chem. C*, 2020, **124**, 11081–11091.
10 A. Yagi, G. Venkataramana, Y. Segawa and K. Itami, *Chem. Commun.*, 2014, **50**, 957–959.
11 K. Senthilkumar, M. Kondratowicz, T. Lis, P. J. Chmielewski, J. Cybinska, J. L. Zafra, J. Casado, T. Vives, J. Crassous, L. Favereau and M. Stepien, *J. Am. Chem. Soc.*, 2019, **141**, 7421–7427.
12 T. A. Schaub, E. A. Prantl, J. Kohn, M. Bursch, C. R. Marshall, E. J. Leonhardt, T. C. Lovell, L. N. Zakharov, C. K. Brozek, S. R. Waldvogel, S. Grimme and R. Jasti, *J. Am. Chem. Soc.*, 2020, **142**, 8763–8775.
13 S. Nishigaki, M. Fukui, H. Sugiyama, H. Uekusa, S. Kawauchi, Y. Shibata and K. Tanaka, *Chem. – Eur. J.*, 2017, **23**, 7227–7231.
14 K. Okada, A. Yagi, Y. Segawa and K. Itami, *Chem. Sci.*, 2017, **8**, 661–667.
15 Y. Segawa, A. Fukazawa, S. Matsuura, H. Omachi, S. Yamaguchi, S. Irle and K. Itami, *Org. Biomol. Chem.*, 2012, **10**, 5979–5984.
16 T. Nishihara, Y. Segawa, K. Itami and Y. Kanemitsu, *J. Phys. Chem. Lett.*, 2012, **3**, 3125–3128.
17 T. Nishihara, Y. Segawa, K. Itami and Y. Kanemitsu, *Chem. Sci.*, 2014, **5**, 2293–2296.
18 N. Oldani, S. K. Doorn, S. Tretiak and S. Fernandez-Alberti, *Phys. Chem. Chem. Phys.*, 2017, **19**, 30914–30924.
19 J. Liu, L. Adamska, S. K. Doorn and S. Tretiak, *Phys. Chem. Chem. Phys.*, 2015, **17**, 14613–14622.
20 M. Fujitsuka, D. W. Cho, T. Iwamoto, S. Yamago and T. Majima, *Phys. Chem. Chem. Phys.*, 2012, **14**, 14585–14588.
21 C. Camacho, T. A. Niehaus, K. Itami and S. Irle, *Chem. Sci.*, 2013, **4**, 187–195.
22 R. Jasti, J. Bhattacharjee, J. Neaton and C. R. Bertozzi, *J. Am. Chem. Soc.*, 2008, **130**, 17646–17647.
23 L. Sicard, F. Lucas, O. Jeannin, P. A. Bouit, J. Rault-Berthelot, C. Quinton and C. Poriel, *Angew. Chem., Int. Ed.*, 2020, **59**, 11066–11072.
24 E. Kayahara, R. Qu, M. Kojima, T. Iwamoto, T. Suzuki and S. Yamago, *Chem. – Eur. J.*, 2015, **21**, 18939–18943.
25 Y.-Y. Liu, J.-Y. Lin, Y.-F. Bo, L.-H. Xie, M.-D. Yi, X.-W. Zhang, H.-M. Zhang, T.-P. Loh and W. Huang, *Org. Lett.*, 2016, **18**, 172–175.
26 L. Sicard, O. Jeannin, J. Rault-Berthelot, C. Quinton and C. Poriel, *ChemPlusChem*, 2018, **83**, 874–880.
27 S. Li, M. Aljhdli, H. Thakellapalli, B. Farajidizaji, Y. Zhang, N. G. Akhmedov, C. Milsmann, B. V. Popp and K. K. Wang, *Org. Lett.*, 2017, **19**, 4078–4081.
28 Y. Li, Y. Segawa, A. Yagi and K. Itami, *J. Am. Chem. Soc.*, 2020, **142**, 12850–12856.
29 E. Kayahara, X. Zhai and S. Yamago, *Can. J. Chem.*, 2017, **95**, 351–356.
30 Y. Kuroda, Y. Sakamoto, T. Suzuki, E. Kayahara and S. Yamago, *J. Org. Chem.*, 2016, **81**, 3356–3363.
31 F. Lucas, L. Sicard, O. Jeannin, J. Rault-Berthelot, E. Jacques, C. Quinton and C. Poriel, *Chem. – Eur. J.*, 2019, **25**, 7740–7748.
32 F. Lucas, N. McIntosh, E. Jacques, C. Lebreton, B. Heinrich, B. Donnio, O. Jeannin, J. Rault-Berthelot, C. Quinton, J. Cornil and C. Poriel, *J. Am. Chem. Soc.*, 2021, **143**, 8804–8820.
33 Z.-Q. Jiang, C. Poriel and N. Leclerc, *Mater. Chem. Front.*, 2020, **4**, 2497–2498.
34 C. Poriel, L. Sicard and J. Rault-Berthelot, *Chem. Commun.*, 2019, **55**, 14238–14254.
35 A. C. Grimsdale and K. Müllen, *Macromol. Rapid Commun.*, 2007, **28**, 1675.
36 C. Poriel and J. Rault-Berthelot, *Acc. Chem. Res.*, 2018, **51**, 1818–1830.
37 M. Romain, D. Tondelier, J.-C. Vanel, B. Geffroy, O. Jeannin, J. Rault-Berthelot, R. Métivier and C. Poriel, *Angew. Chem., Int. Ed.*, 2013, **52**, 14147–14151.

 This journal is © The Royal Society of Chemistry 2022

Open Access Article. Published on 12 September 2022. Downloaded on 10/5/2022 9:01:52 AM.
This article is licensed under a Creative Commons Attribution-NonCommercial 3.0 Unported Licence.

38 J.-D. Peltier, B. Heinrich, B. Donnio, J. Rault-Berthelot, E. Jacques and C. Poriel, *ACS Appl. Mater. Interfaces*, 2017, **9**, 8219–8232.
39 J. D. Peltier, B. Heinrich, B. Donnio, O. Jeannin, J. Rault-Berthelot and C. Poriel, *Chem. – Eur. J.*, 2017, **23**, 17290–17303.
40 M. Romain, C. Quinton, D. Tondelier, B. Geffroy, O. Jeannin, J. Rault-Berthelot and C. Poriel, *J. Mater. Chem. C*, 2016, **4**, 1692–1703.
41 T. C. Lovell, C. E. Colwell, L. N. Zakharov and R. Jasti, *Chem. Sci.*, 2019, **10**, 3786–3790.
42 S. Yamago, Y. Watanabe and T. Iwamoto, *Angew. Chem., Int. Ed.*, 2010, **49**, 757–759.
43 T. Iwamoto, Y. Watanabe, Y. Sakamoto, T. Suzuki and S. Yamago, *J. Am. Chem. Soc.*, 2011, **133**, 8354–8361.
44 M. Fujita, O. Sasaki, T. Mitsuhashi, T. Fujita, J. Yazaki, K. Yamaguchi and K. Ogura, *Chem. Commun.*, 1996, 1535–1536.
45 H. Jia, Y. Gao, Q. Huang, S. Cui and P. Du, *Chem. Commun.*, 2018, **54**, 988–991.
46 Z. Sun, T. Mio, K. Ikemoto, S. Sato and H. Isobe, *J. Org. Chem.*, 2019, **84**, 3500–3507.
47 Z. Sun, K. Ikemoto, T. M. Fukunaga, T. Koretsune, R. Arita, S. Sato and H. Isobe, *Science*, 2019, **363**, 151–155.
48 H.-W. Jiang, T. Tanaka, H. Mori, K. H. Park, D. Kim and A. Osuka, *J. Am. Chem. Soc.*, 2015, **137**, 2219–2222.
49 M. Fujitsuka, C. Lu, B. Zhuang, E. Kayahara, S. Yamago and T. Majima, *J. Phys. Chem. A*, 2019, **123**, 4737–4742.
50 E. Kayahara, T. Kouyama, T. Kato and S. Yamago, *J. Am. Chem. Soc.*, 2016, **138**, 338–344.
51 J. Wang, G. Zhuang, Q. Huang, Y. Xiao, Y. Zhou, H. Liu and P. Du, *Chem. Commun.*, 2019, **55**, 9456–9459.
52 M. D. Peeks, T. D. W. Claridge and H. L. Anderson, *Nature*, 2016, **541**, 200.
53 K. Karon and M. Lapkowski, *J. Solid State Electrochem.*, 2015, **19**, 2601–2610.
54 S. Kato, H. Noguchi, A. Kobayashi, T. Yoshihara, S. Tobita and Y. Nakamura, *J. Org. Chem.*, 2012, **77**, 9120–9133.
55 G. Zotti, G. Schiavon, S. Zecchin, J.-F. Morin and M. Leclerc, *Macromolecules*, 2002, **35**, 2122–2128.
56 A. Y. Rogachev, Z. Zhou, S. Liu, Z. Wei, T. A. Schaub, R. Jasti and M. A. Petrukhina, *Chem. Sci.*, 2021, **12**, 6526–6535.
57 E. Kayahara, L. Sun, H. Onishi, K. Suzuki, T. Fukushima, A. Sawada, H. Kaji and S. Yamago, *J. Am. Chem. Soc.*, 2017, **139**, 18480–18483.
58 Y. Xu, B. Wang, R. Kaur, M. B. Minameyer, M. Bothe, T. Drewello, D. M. Guldi and M. von Delius, *Angew. Chem., Int. Ed.*, 2018, **57**, 11549–11553.
59 Q. Huang, G. Zhuang, H. Jia, M. Qian, S. Cui, S. Yang and P. Du, *Angew. Chem., Int. Ed.*, 2019, **58**, 6244–6249.
60 L. Adamska, I. Nayyar, H. Chen, A. K. Swan, N. Oldani, S. Fernandez-Alberti, M. R. Golder, R. Jasti, S. K. Doorn and S. Tretiak, *Nano Lett.*, 2014, **14**, 6539–6546.
61 S. Sumalekshmy and K. R. Gopidas, *J. Phys. Chem. B*, 2004, **108**, 3705–3712.
62 E. J. Leonhardt and R. Jasti, *Nat. Rev. Chem.*, 2019, **3**, 672–686.